

Indigenous development of 320×256 focal-plane array using InAs/InGaAs/GaAs quantum dots-in-a-well infrared detectors for thermal imaging

K. C. Goma Kumari¹, H. Ghadi¹,
D. R. M. Samudraiah² and S. Chakrabarti^{1,*}

¹Department of Electrical Engineering,

Indian Institute of Technology Bombay, Mumbai 400 076, India

²Formerly with Space Applications Centre, Indian Space Research Organisation, Ahmedabad 380 015, India

We report here the indigenous development of a 320×256 infrared focal-plane imager fabricated using an InAs quantum dots-in-a-well heterostructure, whose photoluminescence peak is at 1162 nm and activation energy is 187 meV. We discuss the fabrication and characterization of single-pixel detectors that can measure intersubband spectral responses with peak intensity at $9.3 \mu\text{m}$. Using the fabricated device, infrared images were captured at 50–90 K. Device optimization led to approximately 95% of the pixels in the imaging array being operational and a reasonably low noise equivalent temperature of approximately 100 mK at 50–60 K.

Keywords: Focal-plane arrays, infrared detectors, photoluminescence peak, quantum dots, thermal imaging.

NANOTECHNOLOGY – which deals with the growth and manipulation of materials at the atomic and molecular levels and facilitates the development of materials with specifically designed performance characteristics – is a key state-of-the-art technology being researched and developed worldwide. The Government of India aims to be technologically self-sufficient by developing advanced technologies indigenously. To this end, the Government has established silicon nanotechnology laboratories at prominent academic institutes such as the Indian Institutes of Technology (IITs) and the Indian Institute of Science, Bengaluru. Nanotechnological advances pertaining to III–V compounds facilitate the development of advanced high-performance devices such as infrared focal-plane arrays (IR FPAs), solar cells, lasers and high-speed devices. Quantum dot (QD) or dot-in-a-well (DWELL) IR FPAs are state-of-the-art devices that may help realize miniature sensor systems. III–V compounds have advantages such as high operating temperatures and low dark currents, resulting in their high performance and applicability. Therefore, the Indian Institute of Technology Bombay (IITB), in collaboration with the Indian Space Research Organisation (ISRO), is researching the design and development of III–V compound QD infrared photodetector/DWELL structure-based detectors, with a

focus on GaAs-based QD/DWELL IR FPAs. In this communication, we discuss DWELL heterostructures and the development of a 320×256 FPA IR imager that has reasonably low noise equivalent differential temperature (NEDT).

The electron–hole pairs or excitons are squeezed in a semiconductor crystallite whose radius is smaller than two times its exciton Bohr radius which is of the order of a few nanometres, leading to quantum confinement. QDs have confinement in all three directions whereas quantum wells and quantum wires have confinement in one and two directions respectively. The quantum energy levels can be predicted using the particle-in-a-box model in which the energies of states depend on the length of the box. The characteristics and properties of such materials differ from those of bulk materials. For example, the desired quantum levels of materials can be engineered and realized through appropriate material selection, growth and geometric arrangement. QD structures have been demonstrated to be more feasible for realizing IR detectors than are quantum well and wire structures. The optoelectronic properties of QDs change as a function of both size and shape. The three-dimensional carrier confinement, sensitivity to normal-incidence radiation, and phonon bottleneck in QDs have spurred research interest in QD-based IR detectors^{1,2}. In addition, QD-based detectors offer a tunable detection window (mid to long wavelength), which has numerous applications in such fields as defence, meteorology (e.g. monitoring weather profiles) and medicine (e.g. medical imaging)^{3,4}. The growth and fabrication of QDs can be challenging; nevertheless, device heterostructures with the desired spectral response can be engineered and grown because of technological advances in high-vacuum systems such as molecular beam epitaxy (MBE) and metal–organic chemical vapour deposition (MOCVD)^{5–7}. Further, such structures can be used to fabricate a thermal imaging device – an FPA with the desired pixel resolutions.

The Stranski–Krastanov growth mode with approximately 7% lattice mismatch has been used to grow InAs QDs on GaAs substrates. The performance of devices thus fabricated can be improved through structural modifications, such as embedding dots in thin InGaAs/InAlGaAs capping and realizing DWELL and dot-in-a-double-well structures^{8,9}. For example, the absorption coefficient of QDs can be improved by stacking multiple dot layers. DWELL structures have attracted considerable academic interest because of their high confinement, bias tunability of spectral response and high-temperature operability¹⁰. Moreover, DWELL structures have low dark-current densities at low temperatures, which improves their photocurrent/noise ratio and in turn their detectivity. Therefore, we used DWELLS for developing FPAs.

Many challenges are encountered in the design, development and realization of QD technology, which requires

*For correspondence. (e-mail: subho@ee.iitb.ac.in)

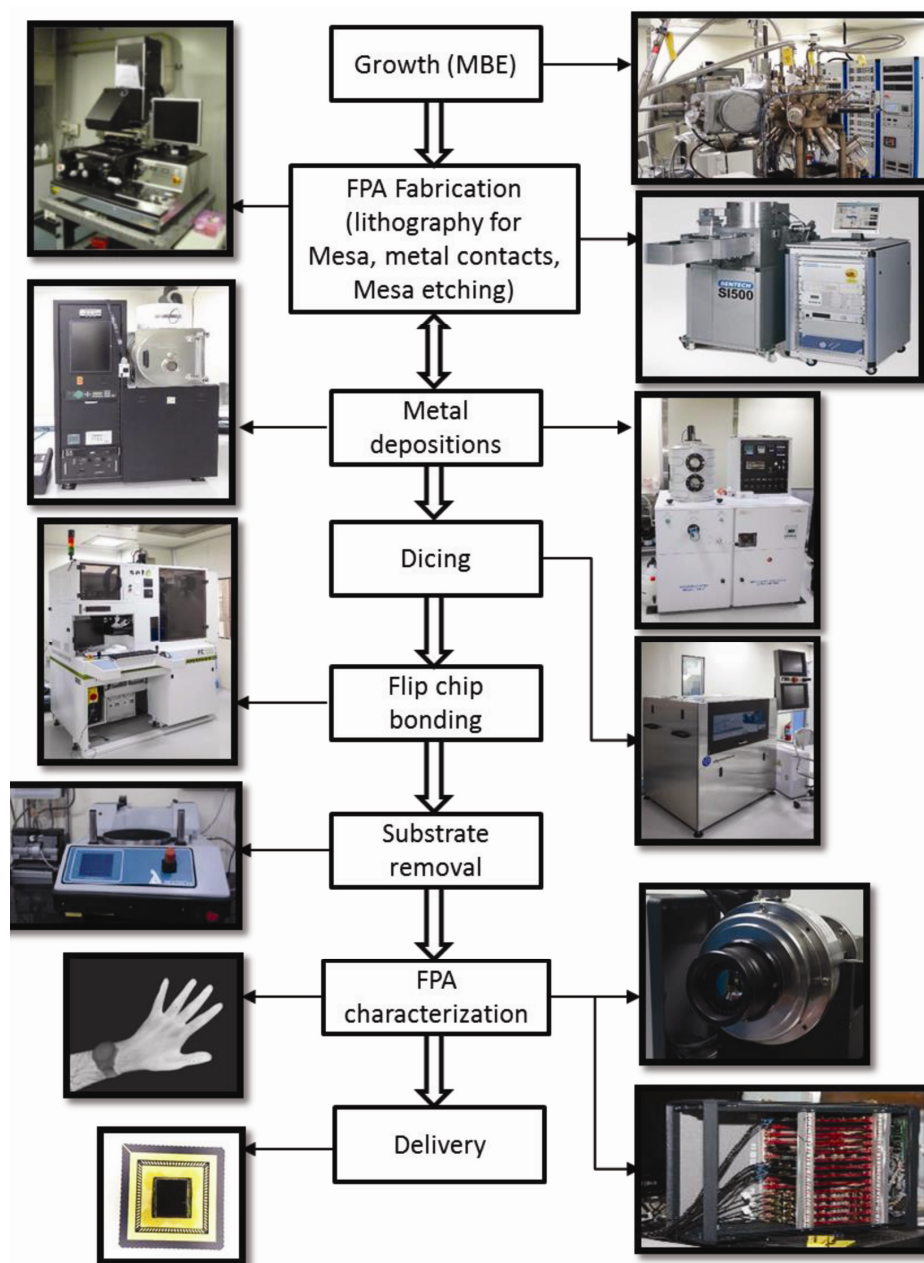


Figure 1. Flow chart of the focal-plane array (FPA) development process showing the capital equipment established under this project (except lithography).

knowledge of QD physics and III–V material technologies as well as access to nanotechnology facilities and equipment. The realization of IR FPAs involves several critical and complex steps, from the growth of the active layers to the packaging of the final device (Figure 1), which was further made difficult because of the lack of indigenous developmental facilities. However, the silicon nanotechnology research experiences at IITB have helped identify and establish various facilities.

For fabricating IR FPAs, a set of masks was designed and realized, and a suitable off-the-shelf silicon readout integrated circuit (ROIC) was selected.

First, QDs were developed through MBE, with the primary goal of realizing the designed structure through appropriate material selection, controlled growth, surface formation using the S–K mode, capping (interface layers) and stacking of structures. Establishing the MBE facility was challenging because it entails multiple ultrahigh vacuum systems, large temperature excursions, multiple sources, and high level of automation and interlock requirements. Through numerous trials to optimize the physical and electro-optical parameters, the facility was tuned for the growth of submonolayers (thickness of 1 monolayer (ML) GaAs is ~ 0.282 nm).

A DWELL heterostructure (Figure 2) was grown on a semi-insulating wafer through solid-source MBE at 500°C. The 2.7 ML InAs QD layer, which is sandwiched between the 2 nm and the 6 nm $\text{In}_{0.15}\text{Ga}_{0.85}\text{As}$ wells, is repeated 10 times with the 50 nm GaAs barrier in each period. The formed dot sizes are about a few tens of nanometres. A highly doped 1000 nm n^+ layer (carrier concentration is $\sim 2 \times 10^{18}$) served as the contact layer. A 50 nm AlAs layer functioned as the etch stop; this protects the active layers from the chemicals used to remove the substrate.

High-energy photons whose energies are higher than that of the band gap of the material are absorbed, thereby raising the electrons from the valence band (VB) to the conduction band (CB). The excited electrons eventually drop to the VB, losing energy by emitting luminescent photons. This process of photon excitation followed by light emission is called photoluminescence (PL). For the measurement of PL, a diced sample was mounted on the cold finger of a closed-cycle liquid-helium cryostat (temperature range, 18–300 K). The mounted sample was excited using a focused beam of a 25 mW 532 nm diode-pumped solid-state laser. The PL signal was collected by lens optics and focused onto the input slit of a 750 mm focal-length spectrometer fitted with a 600 grooves/mm grating blazed at 1 μm ; this signal was detected using liquid nitrogen-cooled 1024-pixel InGaAs detector array.

Photodetectors can be classified as intrinsic and extrinsic detectors. An intrinsic photodetector usually detects light of wavelength close to the bandgap of the semiconductor and creates electron-hole pairs, which induce photocurrent, whereas an extrinsic photodetector can detect light smaller than the bandgap of the semiconductor. In these devices, electron transition corresponds to deep-level impurities and defect levels. When light is

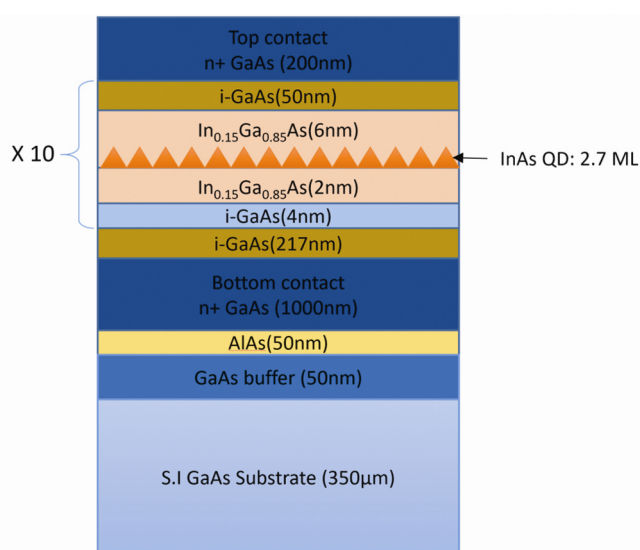


Figure 2. GaAs-based dot-in-a-well (DWELL) heterostructure.

absorbed, an electron is either excited from the deep level to the CB, or it moves from the VB to the deep level by leaving behind a hole in the VB. These excited charge carriers contribute to the photocurrent in their respective bands. Alternatively, extrinsic photodetection also occurs when transition occurs between subband energies. Carrier transition between these subbands, i.e. either the CB or the VB results in absorption and emission at a much higher wavelength. Hence, intersubband transitions can be utilized in IR detectors and emitters.

Single-pixel study aids in the spectral and radiometric characterization of the developed structure before FPA development. To characterize the developed structure, various physical and optical tests – such as microscopic inspection, cross-sectional transmission electron microscopy inspection, electrical testing at various bias voltages and cryogenic temperatures, and spectral response measurements – have been designed and implemented. In the present study, we have developed single-pixel detectors (n - i - n photoconductors) with various optical apertures (100–600 μm) through two-stage lithography using a positive photoresist (S1813). In the first stage, the resist was developed through mesa lithography by UV-exposing the resist in contact with a mesa mask on a double-sided aligner (DSA). The sample was then etched using a wet etchant: phosphoric acid, hydrogen peroxide and deionized water (3 : 1 : 20). Each sample was etched until 10% of the bottom n^+ contact was reached. In the second stage, contact lithography was performed similar to that in the first stage in order to create an opening for metal deposition. The AuGe/Ni/Au metal stack was deposited using a six-target electron-beam evaporator, following which the metal was lifted-off. Subsequently, the device was annealed at 360°C for 90 sec to generate the Ohmic contact. The fabricated single pixels (Figure 3) were fixed on a lead-less chip carrier (LCC), wire-bonded to the pads and characterized. The LCC-mounted device was loaded onto a low-temperature closed-cycle liquid-helium cryostat, and temperature-dependent current-voltage measurements were performed using a source meter (Keithley 2400). The spectral response was measured using a Fourier transform IR spectrometer (ThermoFisher IS50R) fitted with a broadband IR source.

Developing high-performance and highly uniform FPAs is a critical step involving multiple processes, and requires a clean environment and precise machines (Figure 4). Following pixelization, the next major step in FPA development is hybridization using ROIC (i.e. silicon electronics) using indium bumps. Indium bump formation, alignment and fusion are challenging activities that strongly influence pixel uniformity and thus device reliability.

The FPA was fabricated through the three-stage lithography process summarized in Figure 4. In the first stage, the resist was developed through lithography of a 320×256 array of $24 \times 24 \mu\text{m}$ mesa spaced 30 μm apart

using a S1813 positive photoresist, followed by UV exposure on the DSA. Subsequently, by employing the same wet-etching recipe as that used for fabricating the single-pixel devices, the sample was etched until the bottom n^+ layer was reached. In the second stage, an opening was created for metal deposition on each mesa using a AZ5214E image-reversal photoresist. After lithography, AuGe/Ni/Au metal stack was deposited using an e-beam

evaporator, following which the metal was lifted-off using acetone. Next, a thicker photoresist (AZp4620) was used for bump lithography, and a 3 μm -thick indium layer was deposited. After each stage, the sample was visually inspected under a microscope to determine whether it can be further processed. Figure 5 presents the microscopy images of a sample at different stages of fabrication. The FPA device was diced and reflowed with water-soluble reflow flux at 200°C for approximately 60 sec to form an indium bump on each pixel, following which the device was hybridized onto an ROIC chip and under-filled. This underfill imparts the strength necessary to withstand mechanical abrasion (e.g. lapping-polishing) and thermal cycling, and preserves the bonded structure by forming a protective layer around the bonds.

FPA's are back-illuminated devices; therefore, the substrate thickness must be reduced or the substrate eliminated in order to increase the absorption of IR irradiation by the active layers. Substrate removal, which is challenging, was executed using a combination of mechanical lapping-polishing and wet etching. Initially, the substrate was mechanically lapped in the presence of slurry until the thickness was reduced to approximately 80 μm . Then, the substrate was polished to reduce surface roughness, which thinned the substrate to nearly 70 μm . Further mechanical thickness reduction would have resulted in mechanical stress-induced cracking. Therefore, wet chemical etching was conducted using a citric acid-based

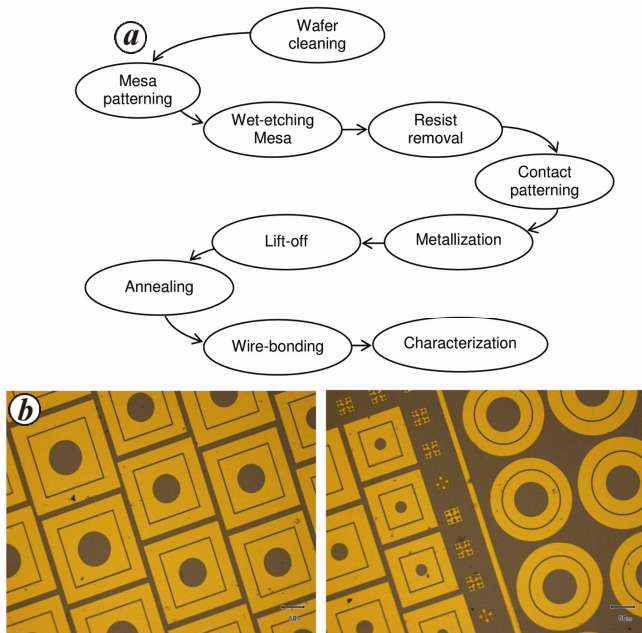


Figure 3. a, Single-pixel device fabrication process. b, images of fabricated single-pixel devices.

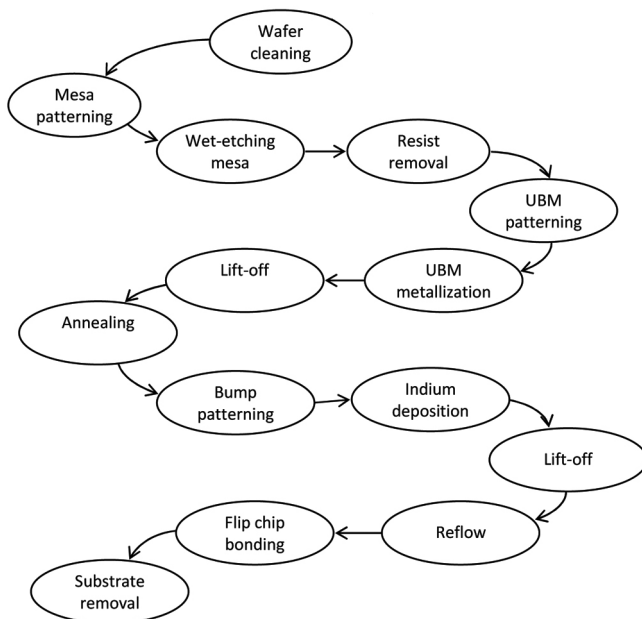


Figure 4. FPA fabrication process showing the various steps of fabrication.

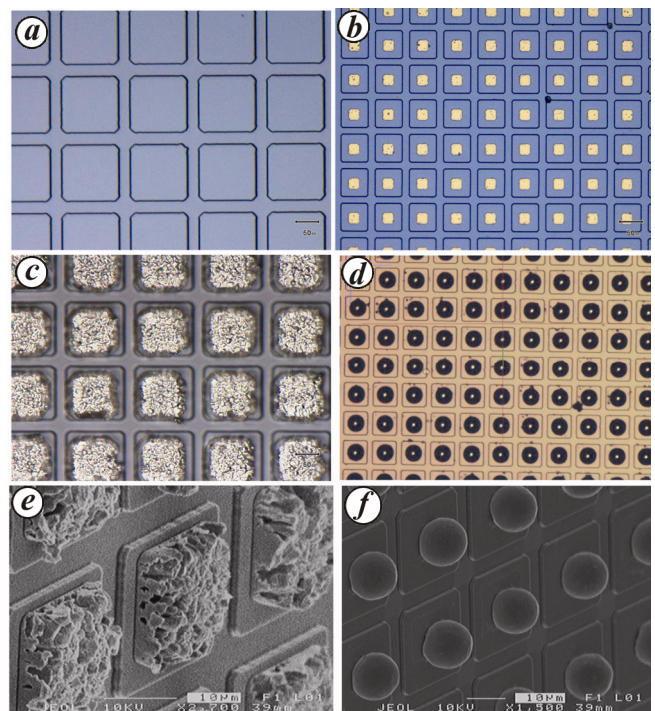


Figure 5. Microscopy images: a, after mesa etching; b, after contact deposition; c, after indium deposition; d, reflow images; e, image of indium pad; f, image of bump.

etchant, which nearly completely removed the GaAs substrate. The etching process was designed such that the reactions ceased on reaching the AlAs layer¹¹. During etching, hydrogen peroxide forms aluminum oxide, which cannot be removed using citric acid unlike oxides of Ga and As. This prevents the etching of the AlAs layer. After substrate removal, the sample was fixed onto a 84-pin LCC, and the ROIC contact pads were wire-bonded. For imaging, the LCC-mounted sample was loaded onto a CamIRA system (SEIR) equipped with single-stage closed-cycle liquid-helium Dewar capable of temperatures as low as 50 K. This system also contains clock cards and a compatible bias card for ROIC.

Figure 6 presents the low-temperature PL spectrum of the DWELL sample obtained through power-dependent PL measurements; the highest peak intensities were at

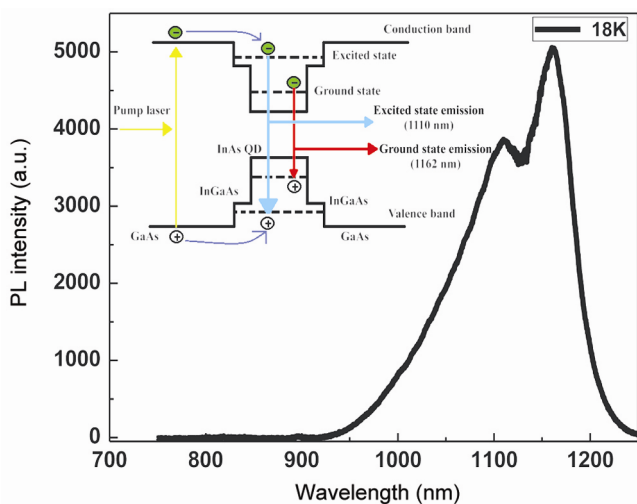


Figure 6. Low-temperature (18 K) photoluminescence (PL) spectrum of the DWELL sample. Inset shows energy-band diagram of a laser-irradiated InAs/InGaAs/GaAs QDIP resulting in various PL peaks.

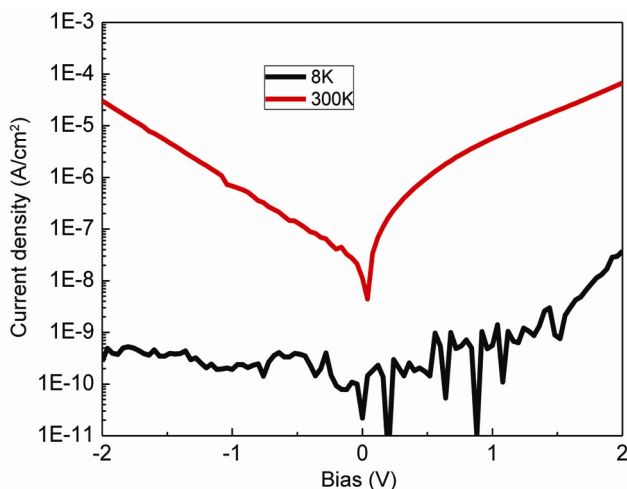


Figure 7. Measured dark-current densities of the DWELL sample at 8 and 300 K.

1162 nm, which correspond to ground-state transition between InAs CB to VB, and at 1100 nm, which correspond to the first excited state transition. PL peaks were observed until 300 K, which indicates the high optical quality of the QD heterostructure, which in turn is attributable to the high carrier confinement in the device. The activation energy was 187 meV, which was determined by

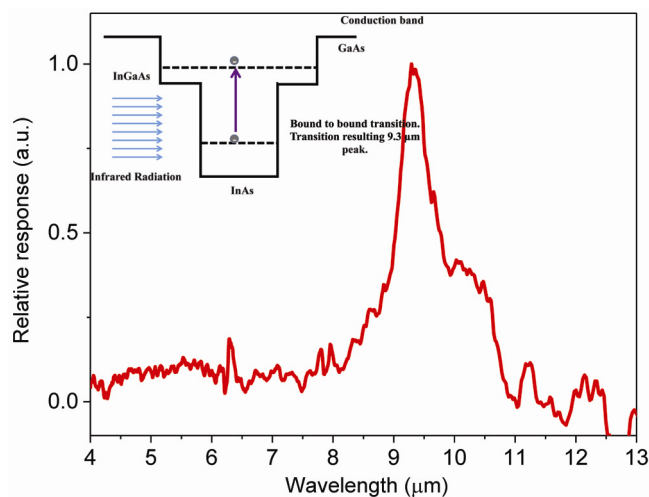


Figure 8. Normalized FTIR intersubband spectral response of the DWELL detector at 80 K. Inset shows proposed model of conduction band explaining peak resulting from intersubband transitions.

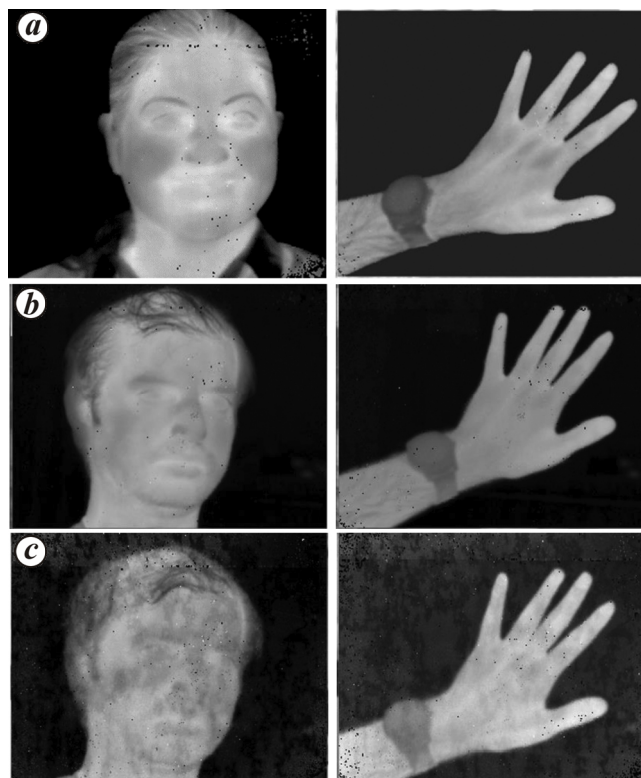


Figure 9. Thermal images captured at (a) 50 K, (b) 60 K and (c) 80 K using the fabricated 320 × 256 FPA.

calculating the area under the ground-state peak through Gaussian fitting and using it in a diode equation. In Figure 7, the room-temperature and low-temperature dark-current densities are compared. The low dark-current density observed from the DWELL sample confirms its suitability for FPA fabrication. The spectral response peak was present at 9.3 μm in the fabricated single-pixel device, which corresponds to the intersubband transition (Figure 8).

Figure 9 shows the thermal images of a person and a hand captured at 50, 60, and 70 K; these images confirm that more than 95% of the pixels are operational. The sample did not exhibit any cracks, mainly because of the successful substrate removal process. NEDT at 50, 60, and 70 K was 103, 103, and 197 mK respectively, which is comparable with those reported in the literature^{9,10,12}. Note that the cited studies have industrial collaborations, whereas the efforts at IITB are only driven by in-house project scientists, master's and doctoral students. Dark current increased at high temperatures, which reduced signal strength, leading to image loss. Future studies can further improve device performance by adding current-blocking layers in the heterostructure. This achievement is a major milestone in indigenous development of DWELL-based IR arrays in India.

Thus, an advanced compound semiconductor research infrastructure was established at IITB to facilitate the indigenous development of nanotechnology-based thermal imaging devices. This advanced facility houses devices such as India's first 4" MBE system, a state-of-the-art flip-chip bonder for back-end integration with readout electronics, an e-beam metallization system, etc. In addition, successful end-to-end trials were completed for all process steps. The developed DWELL heterostructure-based single-pixel detectors exhibited a dominant peak at 9.3 μm and had low dark currents and noise densities. Moreover, we have realized a 320×256 nanotechnology-based FPA capable of capturing images of human targets. An optimization process resulted in more than 95% of the pixels being operational with a reasonably low noise equivalent temperature of 103 mK at 50 K. The device can be optimized further through the same process flow to improve detectivity, which can lead to the realization of thermal imaging at even higher device temperatures. The established facility and the demonstrated technologies have increased the scope for research and development of III–V compounds nanotechnology in India.

dot infrared photodetector. *Appl. Phys. Lett.*, 2007, **90**, 201109(1–3).

4. Jiang, J. *et al.*, Demonstration of a 256×256 middle-wavelength infrared focal plane array based on InGaAs/InGaP quantum dot infrared photodetectors. *Appl. Phys. Lett.*, 2004, **84**, 2232–2234.
5. Williams, J. O., Metal organic chemical vapour deposition (MOCVD) for the preparation of semiconductor materials and devices. In *Growth and Characterisation of Semiconductors* (eds. Stradling, R. A. and Klipstein, P. C.), Adam Hilger, New York, 1990, pp. 17–33.
6. Lundstrom, M., III–V heterojunction bipolar transistors. In *Heterojunction Transistors and Small Size Effects in Devices* (ed. Willander, M.) Studentlitteratur, Sweden, 1992, pp. 35–46.
7. Foxon, C. T. and Joyce, B. A., Growth of thin films and heterostructures of III–V compounds by molecular beam epitaxy. In *Growth and Characterisation of Semiconductors* (eds Stradling, R. A. and Klipstein, P. C.), Adam Hilger, New York, 1990, pp. 35–64.
8. Stiff, A. D., Krishna, S., Bhattacharya, P. and Kennerly, S. W., Normal-incidence, high-temperature, mid-infrared, InAs–GaAs vertical quantum-dot infrared photodetector. *IEEE J. Quant. Electron.*, 2001, **37**, 1412–1419.
9. Andrews, J. R. *et al.*, Comparison of quantum dots-in-a-double-well and quantum dots-in-a-well focal plane arrays in the long-wave infrared. *IEEE Trans. Electron Dev.*, 2011, **58**(7), 2022–2027.
10. Krishna, S., Quantum dots-in-a-well infrared photodetectors. *J. Phys. D*, 2005, **38**, 2142–2150.
11. Broekaert, T. P. E. and Fonstad, C. G., AlAs etch-stop layers for InGaAlAs/InP heterostructure devices and circuits. *IEEE Trans. Electron. Dev.*, 1992, **39**(3), 533–536.
12. Andrews, J. R. *et al.*, Comparison of quantum dots-in-a-well and quantum-well focal plane arrays in the long-wave infrared. *IEEE Trans. Electron. Dev.*, 2009, **56**(3), 512–516.

ACKNOWLEDGEMENTS. We acknowledge the support from the ISRO, Department of Science and Technology and the IIT-B Nanofabrication facility. We are grateful to the Directors of the Space Applications Centre and IIT-B. We are indebted to A. S. Kiran Kumar, Y. S. Sarma, P. Naresh, Arup Banerjee, A. K. Lal, Prof. D. K. Sharma and R. Pinto, all of who contributed at various stages of this research project.

Received 9 September 2016; revised accepted 26 October 2016

doi: 10.18520/cs/v112/i07/1568-1573

1. Ryzhii, V., The theory of quantum-dot infrared phototransistors. *Semicond. Sci. Technol.*, 1996, **11**, 759–765.
2. Gunapala, S. D. *et al.*, 640×512 pixels long-wavelength infrared (LWIR) quantum-dot infrared photodetector (QDIP) imaging focal plane array. *IEEE J. Quant. Electron.*, 2007, **43**, 230–237.
3. Tsao, S., Lim, H., Zhang, W. and Razeghi, M., High operating temperature 320×256 middle-wavelength infrared focal plane array imaging based on an InAs/InGaAs/InAlAs/InP quantum